BALS: Blocked Alternating Least Squares for Parallel Sparse Matrix Factorization on GPUs

Jing Chen, Jianbin Fang, Weifeng Liu, *Senior Member, IEEE* and Canqun Yang

Abstract—Matrix factorization on sparse matrices has been proven to be an effective approach for data mining and machine learning. However, the prior parallel implementations for matrix factorization fail to capture the internal social property embedded in real-world use cases. This article presents an efficient implementation of the alternative least squares (ALS) algorithm called *BALS* built on top of a new sparse matrix format for parallel matrix factorization. The BALS storage format organizes the sparse matrix into 2D tiles to avoid repeated data loads and improve data reuses. We further propose a data reordering technique to sort sparse matrices according to nonzeros. The experimental results show that BALS can yield a superior performance than state-of-the-art implementations, i.e., our BALS generally runs faster than Gates' implementation over different latent feature sizes, with a speedup of up to 2.08× on K20C, 3.72× on TITAN X and 3.13× on TITAN RTX. When compared with alternative matrix factorization algorithms, our BALS consistently outperforms CDMF, cuMF_CCD, and cuMF_SGD over various latent feature sizes and datasets. The reordering technique can provide an extra improvement of up to 23.68% on K20C, 19.87% on TITAN X and 20.38% on TITAN RTX.

Index Terms—Matrix factorization, Alternating least squares, Data reuse, Data reordering, Performance evaluation, GPGPUs

1 Introduction

Matrix factorization has been taken as one of the most successful realizations of latent factor models and thus has been widely used in the machine learning fields such as collaborative filtering recommender systems [8]. Its task is to fill in the missing entries of a partially observed matrix. The input of matrix factorization is an incomplete relation matrix $\mathbf{R}(m \times n)$. In recommender systems, m and n denote the number of users and items, respectively. Due to the sparsity of $\mathbf{R}$, matrix factorization maps both users and items to a joint factor space of dimensionality f (i.e., *latent feature*), so that predicting unknown ratings can be estimated by the inner products of two vectors, x_u of matrix $\mathbf{X}(m \times f)$ and y_i of matrix $\mathbf{Y}(n \times f)$,

$$r_{ui} = x_u {y_i}^T, \tag{1}$$

where x_u denotes the extent of user's interest on items, y_i denotes the extent to which the item owns these factors, and r_{ui} denotes an entry of $\mathbf{R}$. The essence of this problem is to obtain x_u and y_i so that $\mathbf{R} \approx \mathbf{X}\mathbf{Y}^T$. Figure 1 illustrates an example for matrix factorization, where m=n=4 and f=2.

So far, there has been a large amount of work dedicated to the design of fast and scalable methods for large-scale matrix factorization problems [7, 8, 15, 24, 25, 34]. However, matrix factorization over extremely sparse matrices (e.g., recommender datasets) is still a challenging issue [22, 27]. Among the factorization techniques, *alternating least squares* (ALS) has been proved to be an effective one [8]. Compared to *stochastic gradient descent* (SGD) [5, 28], ALS is not only inherently parallel, but can incorporate implicit ratings [8]. Nevertheless, ALS involves sparse matrix manipulation [10] which is challenging to achieve high performance due to imbalanced workload [11], random memory access [17] and task dependency [13]. This particularly holds when parallelizing and optimizing ALS on GPGPUs [3]. For this, researchers have investigated various solutions. Rodrigues *et al.* present a CUDA-based ALS implementation on GPU, which runs faster than the implementation on a multi-core CPU [20]. Tan *et al.* provide a CUDA-based matrix factorization library (*CuMF*), which uses various memory-related techniques to maximize the performance on one or multiple GPUs [26]. Gates *et al.* propose a multi-core CPU implementation and a GPU ALS solver for implicit feedback datasets, which attains good performance through an algorithm-specific kernel and is, thus far, the fastest implementation among these ALS solvers on GPUs [4].

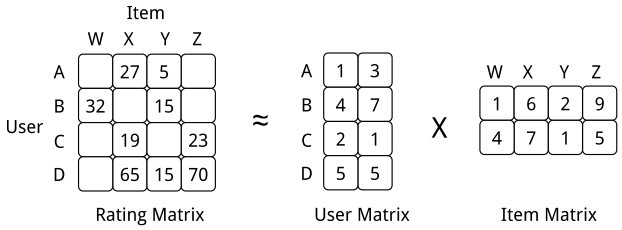

Fig. 1. An example of sparse matrix factorization $\mathbf{R} \approx \mathbf{X}\mathbf{Y}^\mathbf{T}$.

In spite of these efforts, the training speed of parallel sparse matrix factorization based on the ALS algorithm has not reached its optimum. Although the previous works have used fine-grained techniques to exploit the hierarchical resources on modern GPGPUs, they fail to capture and utilize the internal social property embedded in the real-world datasets [3, 7, 26]. This can be drawn from our observation

- *J. Chen, J. Fang and C. Yang are with the College of Computer, National University of Defense Technology, Changsha, China, 410073. E-mail: chjing@chalmers.se, {j.fang, canqun}@nudt.edu.cn*
- *W. Liu is with the Super Scientific Software Laboratory, Department of Computer Science and Technology, China University of Petroleum, Beijing, China, 102249. E-mail: weifeng.liu@cup.edu.cn (Corresponding author: Jianbin Fang and Weifeng Liu.)*

that *there exist many users who have ratings for the same item, and the number of such type of items are enormous in these datasets*. When computing $\mathbf{X}$ or $\mathbf{Y}$, the prior approaches let a thread or a block of threads work on a user vector ($\mathbf{x_u}$) or an item vector ($\mathbf{y_i}$). But updating two user vectors might need the same item vectors from $\mathbf{Y}$. As a result, the same vector would be loaded twice, leading to the redundant data movements and a waste of memory bandwidth. The motivating observations will be detailed in Section 3.

We propose an efficient implementation for parallel sparse matrix factorization, **BALS**[1], based on the alternating least squares algorithm on GPGPUs. BALS aims to avoid repeated data loads of row or column vectors from global memory to shared memory and exploit data reuse based on our observations. For this purpose, we propose a new blocked storage format for sparse matrices by partitioning a matrix into 2D tiles. To enhance data reuse, we further propose a data reordering technique in BALS by sorting rows and columns in the descending order of nonzeros.

The experimental results demonstrate a better performance than the state-of-the-art implementations on three generations of NVIDIA GPUs and six real-world datasets. Overall, BALS runs the fastest among competitive implementations. It outperforms Gates' implementation over different latent feature sizes, with an maximum speedup of 2.08×, 3.72× and 3.13× on K20C, TITAN X and TITAN RTX respectively. We also compare BALS with alternative matrix factorization algorithm implementations, seeing that it outperforms CDMF [32], cuMF_CCD [16] for CCD++ and cuMF_SGD [30] for SGD over different latent feature sizes on these three GPU platforms. Furthermore, data reordering brings averagely extra 8.73%, 8.32% and 10.08% performance improvement over various real-world datasets on K20C, TITAN X and TITAN RTX, respectively. Note that BALS is equally applicable to AMD GPUs, although its implementation is in CUDA and on NVIDIA GPUs.

This paper makes the following contributions.

- We propose a new compressed storage format which organizes a sparse matrix into 2D tiles to facilitate data reuse during matrix factorization.
- We develop a parallel ALS implementation (BALS) on GPGPUs with the storage format to avoid redundant data movements across memory hierarchies.
- We propose a data reordering technique to decrease the processing overhead and further enhance the benefits of data locality.
- We evaluate how BALS performs compared with the baseline implementations on three generations of NVIDIA GPUs and six real-world datasets.

2 Background

This section introduces the ALS-based matrix factorization and analyzes its *time* and *space* efficiency.

2.1 ALS-based Matrix Factorization

Matrix factorization aims to learn the factors by minimizing the regularized squared error on the observed ratings,

1. **BALS** = Parallel **B**locked **ALS** Implementation for Matrix Factorization, and its source code is available at: https://bit.ly/35YUQvW.

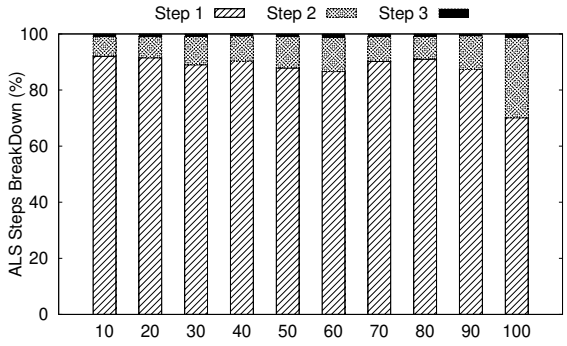

Fig. 2. The illustration about the percentage of three ALS steps on `Netflix` dataset. The three steps are (S1) $\mathbf{Y}^T\mathbf{Y} + \lambda I$, (S2) $\mathbf{Y}^T r_u$, and (S3) solving the linear system.

$$L(X, Y) = \sum_{u,i \in \Omega} (r_{ui} - x_u^T y_i)^2 + \lambda(|x_u|^2 + |y_i|^2), \quad (2)$$

where Ω are the known nonzero ratings of $\mathbf{R}$, and x_u^T are the u^{th} row vectors of the matrix $\mathbf{X}$, y_i are i^{th} column vectors of matrix $\mathbf{Y}$, the constant λ is the regularized coefficient to avoid over-fitting. Therefore, the key to solve this problem is to find approaches of getting the matrices $\mathbf{X}$ and $\mathbf{Y}$.

The minimization principle of alternating least squares is *to keep one fixed while calculating the other*: fixing $\mathbf{Y}$ to calculate $\mathbf{X}$ so as to get vectors x_u, and vice versa. Thus the problem becomes a quadratic function. The procedure iterates until it converges. First, we minimize the equation over $\mathbf{X}$ while fixing $\mathbf{Y}$, and the function becomes

$$L(X) = \sum_{i \in \Omega_u} (r_{ui} - x_u^T y_i)^2 + \lambda |x_u|^2 \quad (3)$$

By calculating the partial derivative of x_u in Function 3 and letting the partial derivative equal zero, we obtain

$$x_u = (Y^T Y + \lambda I)^{-1} Y^T r_u, \quad (4)$$

where I is the unit matrix ranked f, and r_u is the u^{th} rows of $\mathbf{R}$. Likewise, we can obtain

$$y_i = (X^T X + \lambda I)^{-1} X^T r_i. \quad (5)$$

2.2 Algorithm Analysis

The ALS algorithm has three steps, which are (S1) $Y^T Y + \lambda I$, (S2) $Y^T r_u$, and (S3) solving the linear system when updating x_u. As for S1, calculating $\mathbf{Y}^T\mathbf{Y}$ requires $nnz_i \times f \times (f+1)/2$ *multiply-add* operations for a row of $\mathbf{R}$, where nnz_i denotes the number of nonzeros in the current row. Therefore, the total compute cost is $nnz \times f \times (f+1)$, where nnz denotes the total number of nonzeros in $\mathbf{R}$. In terms of memory footprint, we need a matrix $smat$ (sized of $f \times f$) to store the results of $\mathbf{Y}^T\mathbf{Y}$ when updating a row. Thus, the total memory footprint for m rows is $m \times f \times f$. Calculating S2 requires $nnz_i \times f$ *multiply-add* operations when updating the i^{th} row of $\mathbf{R}$. Thus, the total computing cost of S2 is $nnz \times f \times 2$. This step needs a vector $svec$ sized of f to store the results of $\mathbf{Y}^T\mathbf{r_u}$, and thus the total

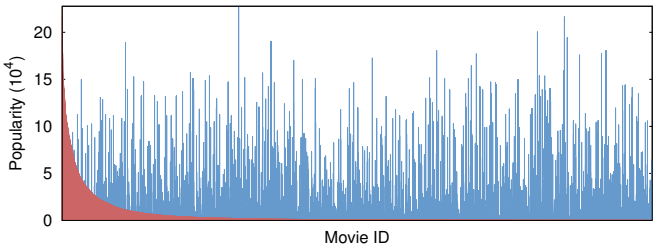

Fig. 3. The illustration about movie popularity among users over the Netflix dataset (blue bars). The red bars demonstrate the popularity of each movie by sorting the matrix according to the number of ratings.

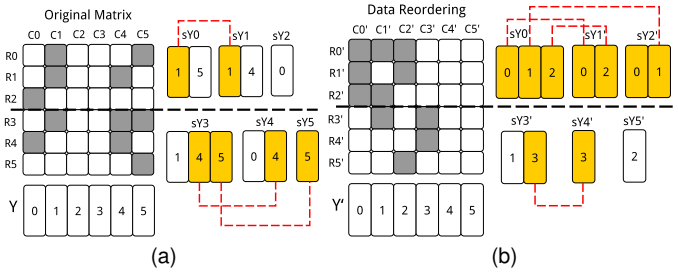

Fig. 4. The illustration of data reuse and the comparison before and after data reordering, where the row block size of the matrix is 3. Matrix $\mathbf{Y}$ denotes the collection of item vectors and $\mathbf{sY}$ is the cached content used to update each user vector.

memory footprint for m rows is $m \times f$. After obtaining $smat$ and $svec$, the *cholesky* decomposition method is exploited to solve the linear system $smat \cdot x_u = svec$ (S3). The time complexity of updating a row of $\mathbf{R}$ is O(f^3).

Figure 2 shows that $\mathbf{Y}^T\mathbf{Y}$ is the most time-consuming step, which takes on average 90% of the end-to-end execution time over various latent factors. Therefore, optimizing this step is the focus of our work. Similarly, calculating $\mathbf{X}^T\mathbf{X}$ takes the most time of updating an item vector (y_i).

3 Motivation

This section starts with our observations coming from the real-world datasets which motive our work.

3.1 Data Reuse

According to our statistics on various recommender datasets, we observe that *there exist popular items which have been rated by the majority of users and, at the same time, there exist users who have given a score to most, if not all, items*. Figure 3 shows the total number of ratings (a.k.a. *popularity*) for each movie of the Netflix dataset. We see that some movies are watched by many users (i.e., the movie has a lot of ratings in one column), while other movies by only a few (i.e., there are very few ratings for the corresponding movie). This is why the diagram shows the vertical sparse lines when the movies are popular.

In alternating least squares, updating a user vector ($\mathbf{x}_u$) needs to load the data elements (i.e., nnz_i column vectors each sized of f) from $\mathbf{Y}$ according to the column indexes of the items that the user has rated. When updating a neighbouring user vector ($\mathbf{x}_{u+1}$), the same column vectors of $\mathbf{Y}$ *may* be used again. This occurs when nonzeros from two distinct rows of $\mathbf{R}$ share the same column index. Thus, we can avoid the movement of one column vector in $\mathbf{Y}$, so as to save the memory bandwidth. Our observation from Figure 3 has shown that this is a common case in recommendation datasets. However, the previous implementations let different threads (or thread blocks) work on distinct user vectors [4, 26]. The already-loaded column vectors from $\mathbf{Y}$ are either evicted out of caches or be manually overwritten in scratch-pad memories. This is the same when we calculate item vectors. In this work, we aim to exploit such a data feature to avoid redundant movements.

Defining data reuse. If there exist two nonzeros of distinct rows sharing the same column index, updating the corresponding row vectors requires the same column vector from $\mathbf{Y}$. Actually, we can avoid one extra data movement of f data elements when updating the row vectors simultaneously. We regard this as a *data reuse*. Analytically, a data reuse occurs once Equation 6 holds.

$$col\_idx[row\_ptr[start_a + i]] = col\_idx[row\_ptr[start_b + j]], \quad (6)$$

where a and b are two rows in a row block of $\mathbf{R}$, i denotes the i^{th} nonzero of row a and j denotes the j^{th} nonzero of row b. In BALS, we organize all rows into groups, each of which is defined as a *row block*. Figure 4a illustrates the concept of *data reuse*, where we group six rows into two row blocks each with three rows. The first nonzero of R0 has the same column index (C1) with the first nonzero of R1. Thus, we only have to load the column vector once (vector 1 shaded in yellow). In the same way, the column vectors (vectors 4 and 5) can be reused in the second row block.

3.2 Data Reordering

Figure 5 shows the nonzero distribution of the six datasets. Each dot of the histogram represents the number of rows with a certain number of nonzeros. We observe that the number of nonzeros varies from very few to tens of thousand, e.g., there are 197,277 rows, each with one nonzero for the YahooMusic R1 dataset. We understand that most elements of the sparse matrix are zeros. Due to the data sparsity, there actually exists many scattered *vacant tiles* and/or *vacant row segments* that are all zeros in specific areas of the rating matrix. Dealing with such vacant segments comes at a cost. If a specific 2D tile is vacant, we only have to check it once and then skip it in the outer iteration. But if there are several vacant row segments in the tile, we have to enumerate the inner iteration to detect these vacant row segments for multiple times, which takes more time than checking a vacant tile. For this, we propose to use a *data reordering* technique by sorting the rows and columns of $\mathbf{R}$ in the descending order of nonzeros. By doing so, many scattered vacant row segments cluster to form new vacant tiles, which reduces the overhead of checking separate vacant row segments.

The red part of Figure 3 shows how the movie ratings distribute of Netflix with data reordering. We see that the popular movies move towards left and leave the unpopular movies on the right. Thus, data reordering can draw the nonzeros to be closer, decrease the number of vacant row segments and create more vacant tiles. Figure 4b illustrates

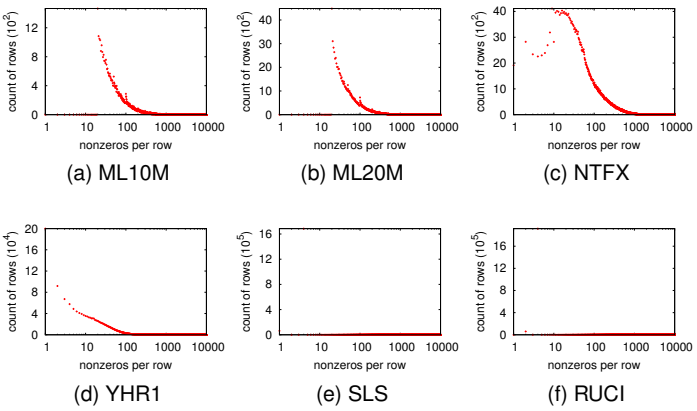

Fig. 5. The nonzero distribution of rows of target datasets.

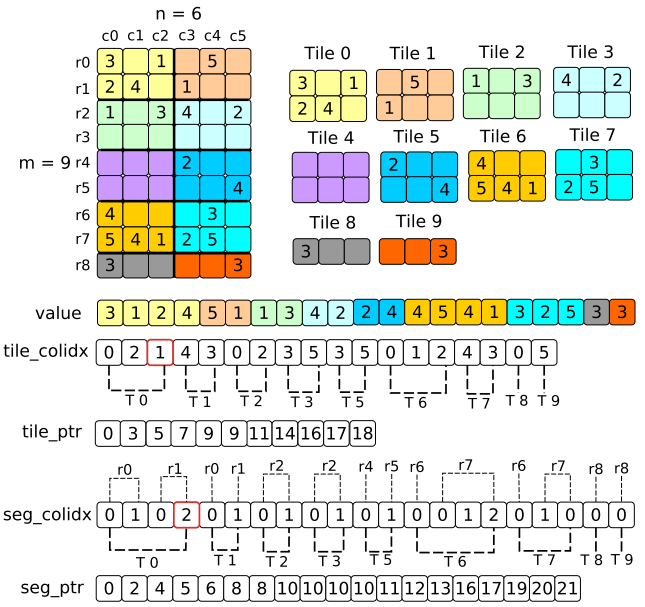

Fig. 6. A sparse matrix $\mathbf{R}$ (9×6) and its BALS data structures.

the data distribution after reordering ratings. Most nonzeros move towards the top-left corner and the total data reuse times increase by 1. Therefore, it is significant to perform data reordering on the rating matrix to enhance data reuse and decrease the processing overhead of vacant segments.

4 BALS Design and Implementation

This section introduces BALS with its data structures and the ALS-based implementation details.

4.1 BALS Storage Format

To exploit data reuse for matrices with any sparsity structures, we organize the sparse matrix into 2D tiles of the same size ($xb \times yb$), where xb and yb denotes the height and the width of a tile, respectively. Thus, BALS has two tuning parameters: xb and yb. To facilitate the ALS computation, BALS uses five data structures: `value`, `tile_colidx`, `tile_ptr`, `seg_colidx` and `seg_ptr`.

Figure 6 shows an example matrix $\mathbf{R}$ with 9 users, 6 items and 21 nonzero elements. We partition $\mathbf{R}$ with xb=2, yb=3, and there are a total of 10 tiles which are differentiated with distinct colors. The `value` array stores all the nonzeros of $\mathbf{R}$, and the size of the array equals the total number of nonzeros. The difference from the conventional CSR format is that we store the nonzeros in a tiled fashion. The other four data structures are illustrated in Sections 4.1.1 and 4.1.2. The pseudocode of how to store rating data with our new data format is shown in Algorithm 1.

4.1.1 Tile Information

We use two `tile` structures (`tile_colidx` and `tile_ptr`) to indicate the column vectors to be loaded for each tile, where `tile_colidx` stores the column indices of the nonzeros within a tile (Lines 10-17 in Algorithm 1) and `tile_ptr` stores the locations in the `tile_colidx` array that start a tile (Lines 10-17 in Algorithm 1).

The `tile_colidx` structure consecutively stores the column indices of each nonzero for the tiles of $\mathbf{R}$. We skip the ones that are redundant across rows of a tile. Note that the indices are the ones in the global space of $\mathbf{R}$, rather than the local space. We regard those columns that have the same column indices in a tile as *redundant columns* and thus record their first appearance only. The array size equals the number of nonzeros in $\mathbf{R}$ minus the number of redundant columns. In Figure 6, there are four nonzeros in tile 0, which are located in three distinct columns (i.e., columns 0, 1 and 2). Among them, the (r0, c0) element, valued 3, shares an identical column index with the (r1, c0) element, valued 2. Therefore, we take the column vector (from $\mathbf{Y}$) indexed by the (r1, c0) element as a *redundant column*. The elements of the `tile_colidx` array are 0, 2, 1 for tile 0. As for tile 1, there exists two nonzeros, i.e., the (r0, c4) element and the (r1, c3) element, shown in Figure 6. Since there is no redundant column in this tile, the following two elements of `tile_colidx` are 4 and 3. In the same way, we can fill `tile_colidx` for the other tiles. In BALS, `tile_colidx` determines which column(s) to load from global memory $\mathbf{Y}$ into shared memory $\mathbf{sY}$. Compared with the implementation in [4], we can avoid loading redundant columns from $\mathbf{Y}$.

The `tile_ptr` structure stores the beginning and ending locations of each tile in `tile_colidx`. Thus, it can be used to determine the starting and the ending indices of the `tile_colidx` array to be visited. Figure 6 shows that the starting index of tile 0 in `tile_colidx` is 0 and the ending address is 2. The size of `tile_ptr` is the number of tiles plus 1. When two adjacent elements in the `tile_ptr` array are identical, we know there is no nonzero in the current tile, which is defined as a *vacant tile*, e.g., tile 4 in Figure 6. Such vacant tiles are skipped when calculating ALS. The last element of `tile_ptr` denotes the number of nonzeros except the redundant ones, which can be used to calculate *redundancy*. Figure 6 shows there are 18 elements except the redundant ones. The redundancy equals the number of nonzeros minus the last element of `tile_ptr`, i.e., $21 - 18 = 3$.

4.1.2 Segment Information

The `tile` structures tell us where to load columns vectors from $\mathbf{Y}$. Then we introduce another two `segment` structures (`seg_colidx` and `seg_ptr`) to indicate the locations of column vectors cached in the high-speed on-chip buffers ($\mathbf{sY}$). Here we refer *a row in a tile* to be as a *segment*.

The `seg_colidx` structure stores the local indices of the nonzeros for each segment (Lines 18-26 in Algorithm 1). This structure allows us to determine which columns we should use in the local buffer ($\mathbf{sY}$). The reason of storing such local indices is that we reorganize column vectors and skip the redundant ones in a tile-wise manner when loading data from global memory ($\mathbf{Y}$) to shared memory ($\mathbf{sY}$). The local indices in `seg_colidx` are actually the tile-scoped locations of the corresponding column vectors in `tile_colidx`. In Figure 6, the (r1, c1) element of $\mathbf{R}$ is of value 4. The global index of the corresponding column vector is located in the third slot (outlined in red) of `tile_colidx`. Thus, the local index of this column vector within the tile is located in the fourth slot (outlined in red) of `seg_colidx`. Each nonzero of $\mathbf{R}$ corresponds to an element of the `seg_colidx` array. Therefore, this array is sized of nnz.

The `seg_ptr` structure stores the starting and the ending locations of each segment in the `seg_colidx` array (Lines 2-9 in Algorithm 1). In Figure 6, the starting index of segment 1 (marked r1 of tile 0) is 2, indicating that the segment starts with the third element in `seg_colidx`. Then we access the corresponding elements in `seg_colidx` and load `seg_colidx[2]` and `seg_colidx[3]`. Meanwhile, we note that the ending index of segment 0 is the starting index of segment 1. When two adjacent elements in `seg_ptr` are identical, we regard that the tile has a *vacant segment*. The size of the array equals $(rows \times segments) + 1$.

Algorithm 1 Storing a Rating Matrix in Our Format

```
1: h ← 0, v ← 1, tile_number ← rows/xb × columns/yb
2: for i ← 0, tile_number do                          ▷ Step1: seg_ptr
3:     for j ← 0, xb do
4:         for k ← row_ptr[j], row_ptr[j + 1] do
5:             seg_colidx[h] ← col_idx[k]
6:             seg_ptr[v] + +
7:         end for
8:     end for
9: end for
10: for i ← 0, tile_number do                         ▷ Step2: tile_ptr, tile_colidx
11:     for j ← seg_ptr[i ∗ xb], seg_ptr[(i + 1) ∗ xb] do
12:         if seg_colidx[j]! = seg_colidx[seg_ptr[i ∗ xb] → j − 1] then
13:             tile_colidx[h] ← seg_colidx[j]
14:             h + +, tile_ptr[i + 1] + +
15:         end if
16:     end for
17: end for
18: for i ← 0, tile_number × xb do                    ▷ Step3: seg_colidx
19:     for j ← seg_ptr[i], seg_ptr[i + 1] do
20:         for k ← tile_ptr[i/xb], tile_ptr[i/xb + 1] do
21:             if seg_colidx[j] == tile_colidx[k] then
22:                 seg_colidx[h] ← k − tile_ptr[i/xb]
23:             end if
24:         end for
25:     end for
26: end for
```

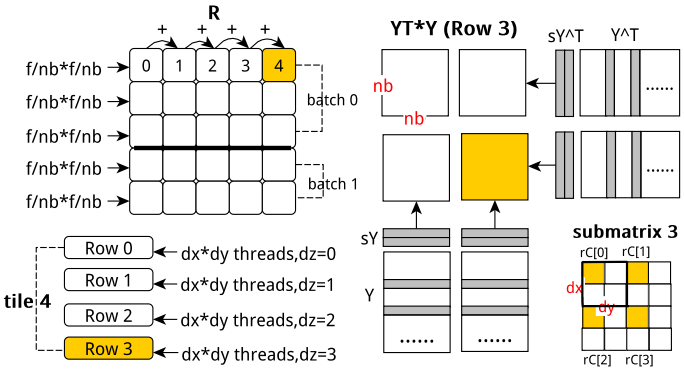

Fig. 7. Illustration of threads configuration of BALS. $\mathbf{R}$ is partitioned into two batches, each of which is divided into multiple 2D tiles.

4.2 BALS Implementation

4.2.1 Work Partitioning and Thread Mapping

BALS uses a batched implementation and updates $batch$ rows one time. As shown in Figure 7, each batch of $\mathbf{R}$ is partitioned into 2D tiles, sized of $xb \times yb$, which are stored in our BALS format (Section 4.1). Each tile contains multiple row segments, and the temporary result ($\mathbf{Y}^T\mathbf{Y}$) for each row segment is stored in an $f \times f$ matrix. The overall temporary results for each row will be accumulated from different segments of the row.

Overall, we partition the $\mathbf{sY}$ ($\mathbf{Y}$) column vectors into subvectors sized of nb. In this case, the $f \times f$ matrix $\mathbf{Y}^T\mathbf{Y}$ is divided into $(f/nb) \times (f/nb)$ submatrices, each sized of $nb \times nb$. We use a 3D grid of thread blocks: $(f/nb, f/nb, tb)$, where $(f/nb) \times (f/nb)$ thread blocks are used to deal with the computing task of a row block, as Figure 7 shows. A row block can be further divided into a row of 2D tiles. The third dimension of the thread-block configuration is tb, which corresponds the number of row blocks of a batch. Meanwhile, a 3D grid of thread configuration is exploited to work on a single tile: (dx, dy, dz), where $dx \times dy$ threads are employed to update a row segment of a tile and dz corresponds to the number of row segments in the tile. Note that dz is limited by the maximum number of threads per block (1024). For instance, when dx=dy=4, the maximum number of dz is 64. Thus, BALS can execute 64 rows of a tile concurrently in this case. In Figure 7, we assume that f=8, nb=4, dx=dy=2. The first batch of $\mathbf{R}$ is partitioned into 3×5 tiles. Thus, we exploit (2, 2, 3) thread blocks in this example. The way of mapping a block of threads to a single tile is shown in the left bottom of Figure 7. There are a total of (2, 2, 4) threads in a block and every 2×2 threads are spawned to work on a row segment.

4.2.2 Implementation Details

Algorithm 2 shows the BALS implementation, which takes three steps to solve $\mathbf{Y}^T\mathbf{Y}$: (1) loading data into shared memory from global memory (Lines 5-7 in Algorithm 2), (2) calculating $\mathbf{Y}^T\mathbf{Y}$ with the data staged in shared memory (Lines 8-14), and (3) storing results into global memory (Line 17). Figure 8 shows an example of the BALS kernel, where xb=6, yb=6, $nonzeros$=8, f=32 and nb=16.

The first step is to load columns from $\mathbf{Y}$ in global memory to $\mathbf{sY}$ in shared memory. BALS accesses `tile_colidx`

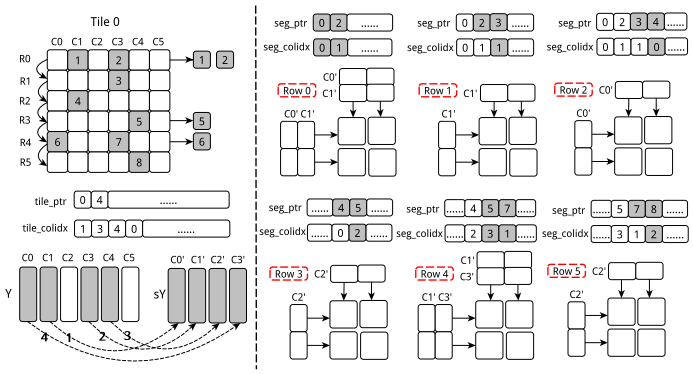

Fig. 8. The schematic view of BALS. The left part of the figure shows how we move data from $\mathbf{Y}$ to $\mathbf{sY}$ by visiting the arrays `tile_ptr` and `tile_colidx`, while the right part illustrates how we compute $\mathbf{sY}^T \cdot \mathbf{sY}$ for each segment with `seg_ptr` and `seg_colidx`.

and `tile_ptr` to determine which columns to load from $\mathbf{Y}$ to $\mathbf{sY}$. We check each row segment of the tile consecutively and obtain the indices of columns to be loaded. For the first row segment in Figure 8, there are two nonzeros having distinct column indices of 1 and 3, respectively. For the second row segment, the nonzero shares the same column index with the second element of the first row segment. Therefore, we only have to load the column vector once into shared memory. In the same way, we enumerate the remaining segments of this tile. By querying `tile_colidx` and `tile_ptr`, we only have to load the column vectors (C0, C1, C3, C4) of $\mathbf{Y}$ into the corresponding slots (C3', C0', C1', C2') of $\mathbf{sY}$. The storing order in shared memory is determined by the element order in `tile_colidx`.

The second step is to calculate $\mathbf{sY}^T\mathbf{sY}$, which is shown in the right part of Figure 8. After obtaining $\mathbf{sY}$, BALS visits the `seg_colidx` and `seg_ptr` arrays to determine which columns of $\mathbf{sY}$ to use for the calculation. There are two elements in the first row segment, so the first and second elements of `seg_ptr` array are 0 and 2, respectively. The `seg_colidx` array stores the local column indices of each nonzero in $\mathbf{sY}$. For example, row segment 0 has two elements, whose column indice corresponds to the first and second columns of $\mathbf{sY}$. Then, we use four thread blocks to calculate $\mathbf{sY}^T\mathbf{sY}$ ($f \times f$ matrix) for each segment of a tile.

Algorithm 2 BALS Implementation

```
1: procedure BALS(Y, xb, yb, data structure; Y^T Y)
2:     tile_number ← columns/yb
3:     for tn ← 1, tile_number do
4:         if tile_ptr[tn + 1] > tile_ptr[tn] then        ▷ Check vacant tile
5:             for c ← tile_ptr[tn], tile_ptr[tn + 1] do   ▷ Load data
6:                 sY[c − tile_ptr[tn]] ← Y[c]
7:             end for
8:             for r ← 0, xb do                            ▷ Calculate sY^T × sY
9:                 if seg_ptr[r + 1] > seg_ptr[r] then
10:                    for k ← seg_ptr[r], seg_ptr[r + 1] do
11:                        r+ = sY[seg_colidx[k]] ∗ sY[seg_colidx[k]]
12:                    end for
13:                end if
14:            end for
15:        end if
16:    end for
17:    Y^T Y ← r                                           ▷ Store temporary results
18: end procedure
```

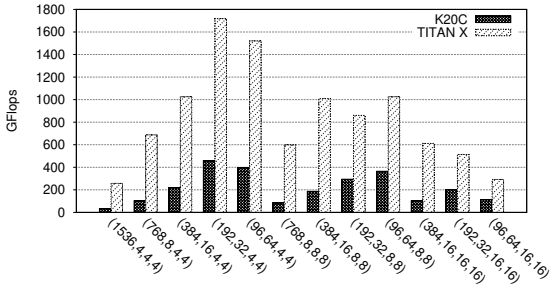

Fig. 9. Selecting the best parameters for BALS of Netflix over two GPU platforms, where f=64, xb=1280. The format of x-axis is (yb, nb, dx, dy).

In BALS, we allocate registers r sized of $nb \times nb \times \lceil xb/dz \rceil$ to store and accumulate the temporary results of all the tiles. The third step is to save the temporary results from r back to the global memory.

4.3 BALS Tile Size Selection

Due to the uneven data distribution of the rating matrix, using BALS will not bring a performance improvement when there is insufficient data reuse in 2D tiles. Thus, we need to pick a right block size of xb and yb for the tiles of a given sparse matrix. Through running a large number of experiments, we observe that BALS can achieve its best performance when *nb is the greatest common divisor of f and dx (dy) is the lowest common multiple (greater than 2) of f*.

On the other hand, the parameter yb is dependent on nb and the size of shared memory. For instance, there are 48-KB shared memory on K20C and each element sized of `float` takes up four bytes. Therefore, the maximum value of yb is 192 when f=64 and nb=32. In this case, we use four thread blocks to deal with the $f \times f$ matrix and need to allocate two local buffers $\mathbf{sY1}$ and $\mathbf{sY2}$. That is,

$$48KB/(4B \times 2 \times 32) = 192.$$

However, for this problem, the choice yb=192 does not yield the best performance. We argue that a larger on-chip memory will lead to a better performance. Figure 9 shows the performance when using various tile configurations on two GPUs (both with 48KB shared memory). We observe that yb=192, nb=32 and dx=dy=4 is the best configuration while f=64, xb=1280 on both K20C and TITAN X.

4.4 Data Reordering

By reordering rows or columns according to the number of nonzeros in each row or column, the nonzeros will walk towards the top-left corner of the rating matrix. Thus, we can further increase the benefits of data reuse, and eliminate the overhead of processing vacant segments. Algorithm 3 demonstrates how we reorder rows.

The inputs of data reordering algorithm are the original rating matrix $\mathbf{R}$ in the conventional CSR format. The output is the reordered matrix $\mathbf{R}'$ represented with three updated data structures (dr_value, dr_rowptr, and dr_colidx). We first initialize the intermediate variables and the temporary arrays to be zero. Then, we obtain the longest row according to the nonzeros of each row in $\mathbf{R}$ by calculating $row\_ptr[u+1] - row\_ptr[u]$. After that, we store its information into

Algorithm 3 Data Reordering

procedure DATA REORDERING(R (val, row_ptr, col_idx); R' ($dr\_val, dr\_rowptr, dr\_colidx$))
  $dr\_val, dr\_rowptr, dr\_colidx, h \leftarrow 0$
  for $u \leftarrow 1, m$ **do**
    $find\ longest\ row\ lr \leftarrow row\_ptr[u+1] - row\_ptr[u]$
    for $i \leftarrow row\_ptr[lr], row\_ptr[lr+1]$ **do**
      $dr\_val[h] \leftarrow value[i]$
      $dr\_colidx[h] \leftarrow col\_idx[i]$
      $h++$
    end for
    $dr\_rowptr[u+1] \leftarrow dr\_rowptr[u] + length$
    $length\ of\ lr \leftarrow -1$
  end for
end procedure

three temporary arrays, including nonzero values, col_idx and row_ptr of this row. The final step is to reinitialize the number of nonzeros in this longest row to be -1. In this way, we can leave it out in the next iteration and obtain the second longest row in the matrix. Reordering columns can be performed in a similar way.

5 Experimental Setup

This section introduces the hardware and software platforms, and describes the real-world recommender datasets.

GPU Hardware and Software. NVIDIA Tesla K20C GPU, TITAN X Pascal and TITAN RTX Turing are utilized for the following experiments. Tesla K20C contains 13 streaming multiprocessors (SM), each with 192 CUDA cores. The theoretical peak floating point performance of K20C is 3.52 Tflops in single precision and 1.17 Tflops in double precision. TITAN X Pascal has 3840 CUDA cores spread across 30 streaming multiprocessors (SM) and six graphics processing clusters (GPCs) from which 3584 are enabled on the TITAN X Pascal. TITAN RTX Turing includes 4608 CUDA cores across 72 SMs, 576 Tensor cores, 72 RT cores, 288 texture units, and 36 PolyMorph engines. Not only does Titan RTX sport more CUDA cores than GeForce RTX 2080 Ti, it also offers a higher GPU Boost clock rating (1,770 MHz vs. 1,635 MHz). As such, its peak single-precision rate increases to 16.3 Tflops. Besides, we use `CUDA v7.5` for K20C, `CUDA v8.0` for TITAN X and `CUDA v10.2` for TITAN RTX respectively, which is taken as the communication backbone between CPU and GPU.

Input Datasets. We use six datasets (`Movielens 10M`, `Movielens 20M`[2], `Netflix`[3], `YahooMusic R1`[4], `Sls`, `Rucci`[5]) to evaluate the ALS performance. The format of each dataset is $(userID, itemID, rating)$. We pre-process each dataset according to this format. The details of the datasets are shown in Table 1. Note that m is the number of users, n is the number of items, and nnz is the number of the nonzero entries in the rating matrix $\mathbf{R}$. The sparsity of a rating matrix is calculated by $nnz/(m \times n)$. In the experiments, the nonzero entries are in single precision.

Competitive Approaches. *Rodrigues et al.* introduce a basic ALS implementation in CUDA [20], where each GPU thread updates a row x_u of $\mathbf{X}$ (Equation 4) or a column y_i of $\mathbf{Y}$ (Equation 5). Thus, the implementation has a total of m (or n) independent tasks and at most m (or n) threads can run concurrently. As one GPU thread is used to update a row of the $\mathbf{X}$ matrix, all the temporary data of $\mathbf{Y}^T\mathbf{Y}$ is allocated dynamically in the kernel function. However, when f becomes large, there is insufficient global memory space remained for dynamic allocation and thus the kernel failed to run. Therefore, the implementation does not scale well over the latent factor. Given that their work is a baseline implementation and only supports f=10, we only compare other three ALS implementations in this section.

CuMF uses a thread block to update a row of the $\mathbf{X}$ matrix or a column of the $\mathbf{Y}$ matrix [26]. The entire task of calculating $\mathbf{Y}^T\mathbf{Y}$ is partitioned into multiple tiles, each sized of 10×10. Then CuMF lets each thread work on such a data tile. Instead of using a loop to iterate a 10×10 data tile, it fully unrolls the loop and allocates 100 registers to store the temporary results of $smat$. Taking f=10 as an example, CuMF uses only one thread to calculate the temporary results of $\mathbf{Y}^T\mathbf{Y}$.

Gates et al. present an ALS solver in CUDA [4]. They leverage a batched implementation and use a 3D grid of thread blocks, $(\lceil \frac{f}{nb} \rceil, \lceil \frac{f}{nb} \rceil, batch)$. The product of $\mathbf{Y}^T\mathbf{Y}$ is an $f \times f$ matrix for each row of $\mathbf{R}$, and this task is divided into sub-tiles sized of $nb \times nb$. Each sub-tile is mapped to a thread block. The approach moves the corresponding columns of $\mathbf{Y}$ sized of $kb \times f$ into shared memory $\mathbf{sY}$ (or $\mathbf{sY^T}$) and exploits $(f/nb) \times (f/nb)$ thread blocks to calculate $\mathbf{Y}^T\mathbf{Y}$. Meanwhile, they use a 2D grid of thread configuration (i.e., each thread block has $dx \times dy$ threads) and allocates a register file sized of $(nb/dx) \times (nb/dy)$ for each thread to save the temporary results.

TABLE 1
The recommender datasets.

	Acronym	m	n	nnz	sparsity
Movielens 10M	ML10M	71567	65133	8000044	0.0017
Movielens 20M	ML20M	138493	27278	20000263	0.0053
Netflix	NTFX	480189	17770	99072112	0.0116
YahooMusic R1	YMR1	1948882	98212	115248575	0.0006
Sls	SLS	1748122	62729	6804304	6.21e-5
Rucci	RUCI	1977885	109900	7791168	3.58e-5

6 Performance Evaluation

This section reports how well BALS performs, by comparing BALS with the state-of-the-art ALS implementations, and evaluating the performance impact of the reordering techniques and BALS tuning parameters.

6.1 Comparison to State-of-the-Art Implementations

Figure 10 presents the comparison with other two state-of-the-art ALS implementations (*Gates'* and *CuMF*) over different f (ranging from 10 to 100) on six datasets. BALS generally runs the fastest among the three implementations and Gates' implementation runs the second on the three GPUs. Specifically, our BALS implementation runs, on average, 1.26×, 1.46×, 1.30×, 2.19×, 2.30× and 2.25× faster than Gates' for `Movielens 10M`, `Movielens 20M`, `Netflix`, `Yahoomusic R1`, `Sls` and `Rucci` on K20C, respectively.

2. http://files.grouplens.org/datasets/movielens/
3. http://www.select.cs.cmu.edu/code/graphlab/datasets/
4. http://webscope.sandbox.yahoo.com
5. http://www.cise.ufl.edu/research/sparse/matrices/

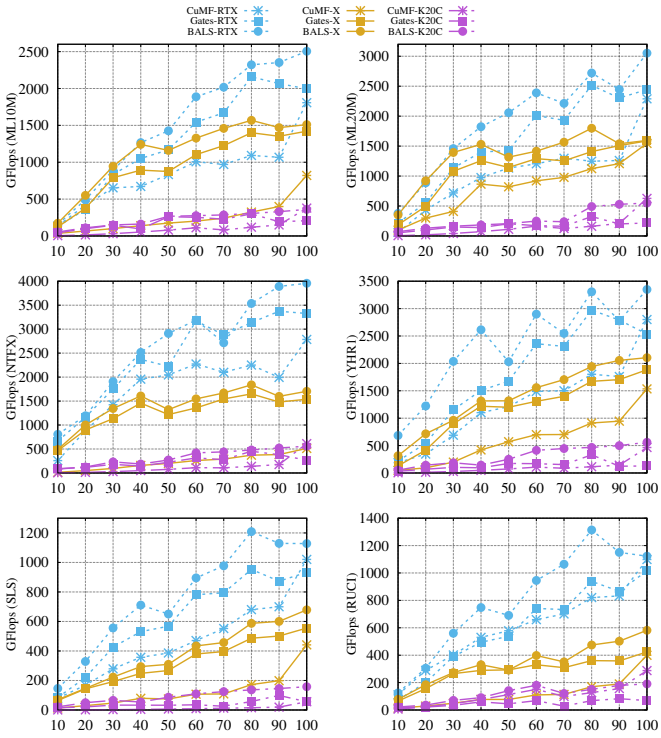

Fig. 10. Performance comparison of three ALS implementations with f ranging from 10 to 100 on three GPUs.

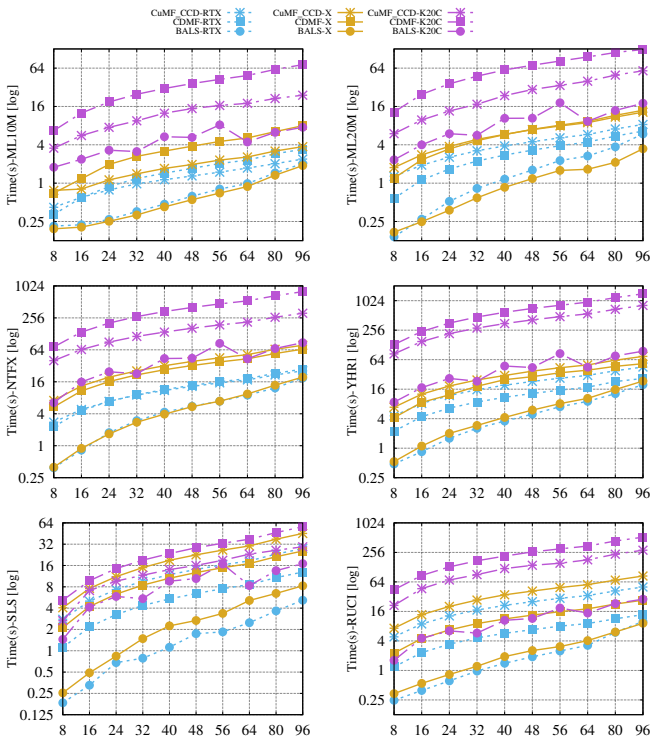

Fig. 11. Performance comparison of CDMF, CuMF_CCD and BALS, where we keep the same RMSE in this case.

TABLE 2
The speedup of BALS over CDMF and CuMF_CCD (x)

Platform	Comparison	ML10M	ML20M	NTFX	YHR1	SLS	RUCI
K20C	vs. CDMF	7.10	6.89	9.37	15.26	3.04	21.64
	vs. CuMF_CCD	2.75	2.31	4.04	9.09	1.79	11.39
X	vs. CDMF	6.13	6.64	7.35	5.21	5.39	5.79
	vs. CuMF_CCD	3.50	7.18	9.01	7.28	9.68	17.88
RTX	vs. CDMF	2.51	2.44	3.13	3.04	4.45	3.80
	vs. CuMF_CCD	2.09	3.86	3.22	5.53	10.03	14.40

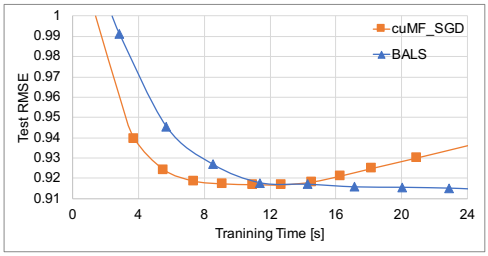

Fig. 12. Converge speed comparison between cuMF_SGD and BALS (each blue triangle dot represents a single ALS iteration, while each red square dot represents 10 SGD iterations).

The performance improvements (geometric mean) of BALS over Gates' implementation reach 24%, 28%, 11%, 28%, 15% and 19% on TITAN X, and 20%, 30%, 11%, 49%, 31% and 39% on TITAN RTX on these six datasets, respectively.

When f is small, the performance gap between BALS and Gates' implementation over various datasets is small. But when f increases, the performance gap becomes larger. This is because a larger f allows for better data reuse, e.g., BALS achieves the maximum speedup of 4.38× over *Gates*' when f=100 on K20C for `YahooMusic R1`. Note that CuMF exploits a specially customized kernel for the case when $f = 100$, which leads to a dramatic performance improvement.

6.2 Comparison to SGD and CCD++

This section compares BALS with three state-of-the-art CCD and SGD implementations: CDMF [32], cuMF_CCD [16] for CCD++ and cuMF_SGD for SGD [30].

Figure 11 shows the performance comparison of CDMF, cuMF_CCD and BALS over different latent feature sizes (from 8 to 96) on K20C, TITAN X and TITAN RTX. We observe that BALS outperforms CDMF and CuMF_CCD over different latent feature sizes on six datasets, while not changing the prediction accuracy (i.e., RMSE). We see that CDMF and CuMF_CCD scale linearly, while BALS fluctuates slightly due to the different best observed parameters chosen for different f. Table 2 lists the average speedups of BALS over CDMF and CuMF_CCD, which shows different level of performance speedups on six datasets.

We also compare BALS to cuMF_SGD when f=128. The performance results (in terms of GFlops) show that BALS achieves an average speedup of 5.3× (5.6×) over six datasets on TITAN RTX (K20C), compared to cuMF_SGD. Figure 12 shows the RMSE comparison with regards to the training time on TITAN RTX with *Netflix* dataset. Since ALS requires more computations per iteration, it runs slower than SGD. We also see that, the execution time of a single BALS iteration equals to that of 4–5 cuMF_SGD iterations. On the other hand, BALS requires fewer iterations to coverage than cuMF_SGD. That is, BALS converges with around 5 iterations, whereas cuMF_SGD requires around 40 iterations to achieve the same RMSE.

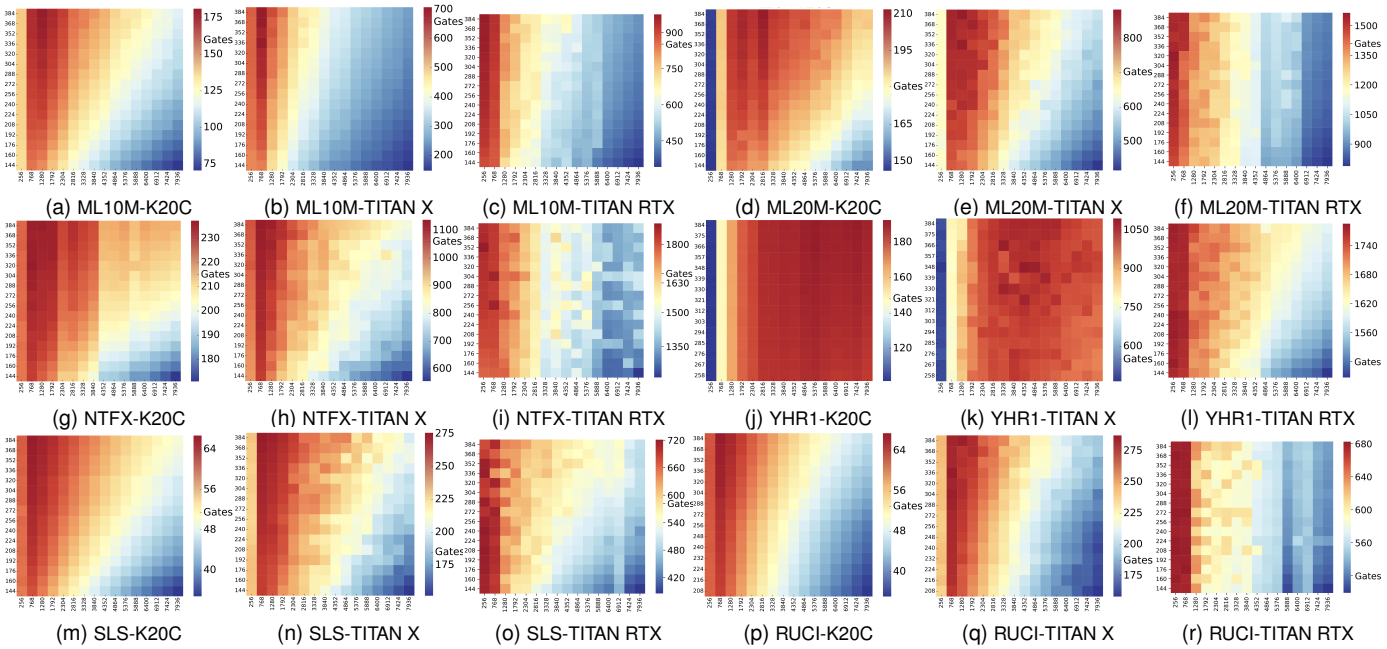

Fig. 13. The performance impact over xb and yb and the performance comparison (GFlops) of BALS and Gates' implementation (labeled on the colorbar) before data reordering on various datasets, where f=32, nb=16, dx=dy=4. X-axis is xblock, from 256 to 7936, step increase is 512. Y-axis is yblock, from 144 to 384, step increase is 16. A more visible version is available at: https://bit.ly/35YUQvW.

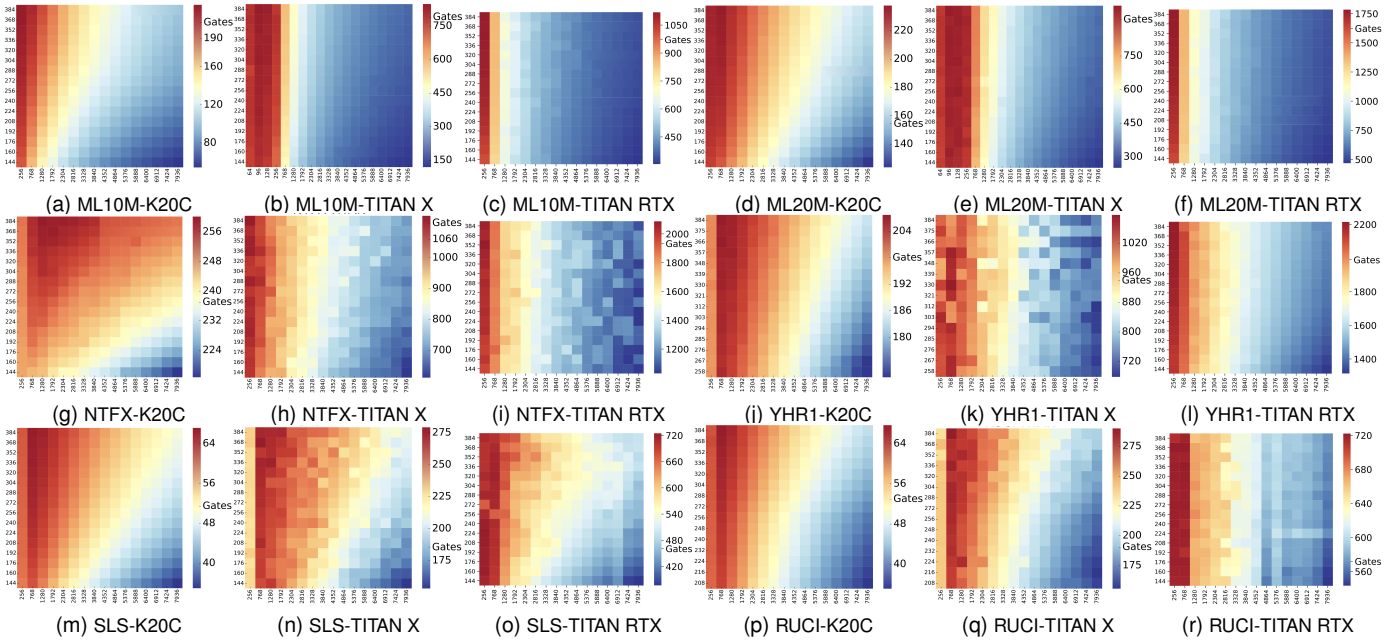

Fig. 14. The performance impact over xb and yb and the performance comparison (GFlops) between BALS and Gates' implementation (labeled on the colorbar) after data reordering on various datasets, where f=32, nb=16, dx=dy=4. X-axis and y-axis keep the same as Figure 13. A more visible version is available at: https://bit.ly/35YUQvW.

6.3 Impact of xb and yb

The tile size xb and yb have a dramatic performance impact on BALS, which determines the data reuse. Figures 13 shows the performance impact of xb and yb on various datasets and three GPUs. BALS's performance changes gradually with xb and yb, and the best tile size typically appears on the top-left corner of heatmaps. Theoretically, for a fixed yb (xb), the data reuse linearly increases with xb (yb). However, in order to achieve the best performance in BALS, it is necessary to balance the benefit from column reuse and the computing cost due to increased number of rows in a specific tile. As Figure 13 heatmaps show, the performance changes from red to blue in most of cases when xb increases, which indicates that the calculation cost caused by increasing xb overtakes the benefit of data reuse. Also, this observation hints best parameter choices. Note that there exists a dramatic performance change for `Movielens 20M` and `YahooMusic R1` on K20C and TITAN X, when xb ranges from 256 to 1280, whereas this change is minor on TITAN RTX. This comes from these datasets differing from

TABLE 3
The percentage of vacant tiles and segments and performance gain

	Before Reordering			After Reordering		
	Vacant Tiles	Vacant Segments	Benefits	Vacant Tiles	Vacant Segments	Benefits
ML10M	43.67%	49.44%	11.88%	87.92%	7.82%	16.22%
ML20M	18.30%	63.85%	7.51%	27.81%	57.36%	0.25%
NTFX	2.38%	24.10%	0	0.59%	69.59%	0.15%
YHR1	52.28%	45.73%	23.65%	81.13%	17.31%	7.13%
SLS	26.35%	71.85%	9.04%	19.35%	79.07%	13.31%
RUCI	72.32%	26.92%	60.37%	72.95%	26.29%	41.60%

TABLE 4
The performance improvements of data reordering

	ML10M	ML20M	NTFX	YHR1	SLS	RUCI
K20C	23.68%	11.72%	9.77%	6.26%	0.64%	0.33%
TITAN X	19.87%	11.92%	8.96%	5.87%	1.29%	2.02%
TITAN RTX	14.67%	14.07%	10.35%	20.38%	0.83%	0.18%

the rest. The first few rows of the two datasets have so few nonzeros that the tiling benefits cannot offset the overhead.

The performance of *Gates'* implementation [4] is labeled on the colorbar of Figure 13. We see that BALS can outperform Gates' implementation over various datasets on K20C, TITAN X and TITAN RTX. The performance improvements on TITAN RTX based on Gates' implementation are upto 14.6%, 9.3%, 13.2%, 38.6%, 23.9% and 53.2% for `Movielens 10M`, `Movielens 20M`, `Netflix`, `Yahoomusic R1`, `Sls` and `Rucci`, respectively. And BALS obtains the largest performance improvement (by 99%) on TITAN X for `YahooMusic R1` when f=32, while using the same configuration can achieve only half of that on K20C. For `Sls` and `Rucci`, BALS achieves an average performance improvement of 49.2% on TITAN X and 29.8% on K20C compared to Gates' implementation.

6.4 Vacant Tiles and Segments Analysis

The rating matrix $\mathbf{R}$ is divided into multiple 2D tiles in BALS. Due to the sparsity of $\mathbf{R}$, there exists a large amount of vacant tiles/segments. Thus, we introduce an inspection mechanism of identifying vacant tiles/segments. We count the percentage of vacant tiles and segments of the six datasets and measure the performance benefits of skipping them when f=32 (Table 3). Note that we differentiate the vacant tiles and vacant segments, i.e., those segments within a vacant tile are excluded from pure vacant segments. We see that the vacant tiles and vacant segments occupy a large percentage in rating matrices, with an average 35.88% of vacant tiles and 46.98% of vacant segments before reordering in the six datasets. As a result, we obtain various levels of performance improvement when skipping these vacancy. Using the inspection mechanism yields the largest performance improvement of 60.37% `Rucci`, while the gain is very little for `Netflix`. This is because `Netflix` is a denser matrix among the recommender datasets, whose sparsity is shown Table 1). The percentages of vacant tiles and vacant segments are much less than those of other datasets.

6.5 Impact of Data Reordering

BALS clusters the nonzeros of the rating matrix to exploit data locality with the data reordering technique. Table 3 shows that the proportions of vacant tiles and segments change significantly after reordering. The percentages of vacant tiles for most datasets are larger, while the percentages of vacant segments drop except `Netflix` and `Sls`. When the nonzeros cluster as much as possible, the scattered vacant segments without reordering form new vacant tiles, and thus we have more vacant tiles and fewer vacant segments with the reordering technique.

Figures 13 and 14 show the performance impact of data reordering. First, the performance (xb,yb) configurations (red) move towards the left parts after data reordering. Thus, the best tile configuration changes by reordering rows or columns. For `Movielens 10M`, BALS performs the best when xb=1280, yb=384 before reordering on K20C and xb=768, yb=384 on TITAN X, whereas the best configuration is of xb=256, yb=384 after reordering. Second, the best observed tile configuration differs across datasets. The best performance is achieved at xb=2816, yb=384 on K20C before reordering and at xb=768, yb=384 after reordering for `Movielens 20M`. Third, we summarize that achieving the best performance without data reordering requires more rows within a tile to exploit data reuses. Fourth, enlarging xb cannot improve the performance after reordering $\mathbf{R}$, which leads to broader blue fields in Figure 14 compared with Figure 13. This is because most data move to left upper part with reordering, and the data reuse occurs in most left upper part. Therefore, it has much less data and no extra significant data reuse by using a larger xb, which leads to a lower performance.

Our data reordering technique brings further performance improvement, compared to Gates' implementation. Table 4 lists the performance improvements of the data reordering technique over the six datasets in BALS when compared with the performance without data reordering. We obtain different levels of performance improvements, with an average improvement of 8.73%, 8.32% and 10.08% on K20C, TITAN X and TITAN RTX, respectively. The performance improvement for `Movielens 10M` increases by 23.68% on K20C, 19.87% on TITAN X and 14.67% on TITAN RTX. However, we observe that the data reordering technique brings a rather small performance improvement for the `Sls` and `Rucci` datasets. This is because their matrix shape is more structured, and their nonzeros distribute more evenly across rows or columns than the other four datasets.

6.6 Impact of Feature Space Size

The first step of $\mathbf{Y}^T\mathbf{Y}$ is to load corresponding column vectors each sized of f from $\mathbf{Y}$ to s$\mathbf{Y}$. A larger f allows more data to be loaded to on-chip memories. And using BALS can avoid $redundancy \times f$ repeated data loads. As a result, BALS can avoid a large amount of data loads from off-chip to on-chip when f is large. Figure 15 shows the performance impact of the feature space size (f ranging from 8 to 96) on the three platforms. We note the BALS performance trend being mostly independent of the architecture, while there exists a significant difference in the actual performance numbers. We observe minor fluctuations between f=8 to 56 on K20C and TITAN RTX. But after f=56, it is obvious that BALS has a dramatic performance improvements due to more data uses and fewer data loads.

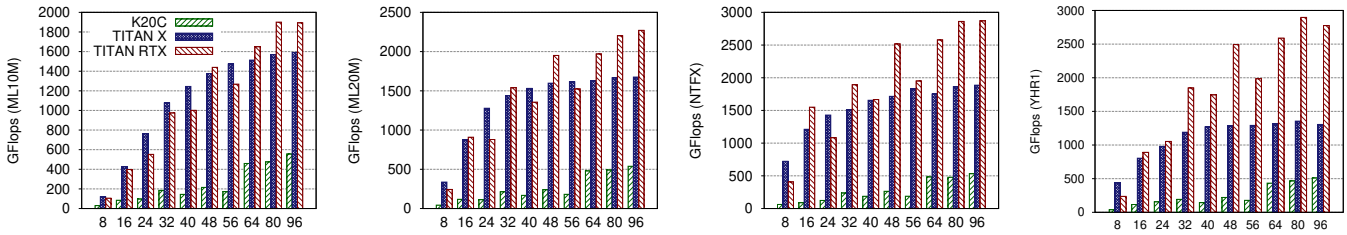

Fig. 15. The performance impact of different f ranging from 8 to 96 on BALS, where xb, yb exploit the best observed parameters from Section 6.3.

7 Related Work

This section discusses four *matrix factorization* algorithms and their state-of-the-art parallel implementations.

The ALS solver. `GraphLab` implements ALS by distributing matrix on multiple machines for large matrices, which results in heavy cross-node traffic and high network bandwidth [12]. `Spark MLlib` leverages partial matrix replication to parallelize ALS [14]. `CuMF` is a CUDA-based matrix factorization library, which implements memory-optimized ALS to solve large-scale matrix factorization on either single or multiple GPUs. Gates *et al.* formulate ALS as a mix of cache-optimized algorithm-specific kernels and batched Cholesky factorization [9], and accelerate it on GPUs and multi-threaded CPUs [4]. Zhou *et al.* introduce a new parallel algorithm ALS-WR (weighted regulation) for large-scale problems by using parallel Matlab on a linux cluster [34].

The CCD solver. Yu *et al.* propose a scalable method (CCD++), which has a different update sequence from the conventional CCD (Cyclic Coordinate Decent) and updates rank-one factors one by one. The algorithm has two parallel implementations: one for multi-core shared memory systems and the other for distributed systems [33]. Recently Nisa *et al.* improve the CCD++ method on GPUs with loop fusion and tiling [16]. Yang *et al.* present an efficient and portable CDMF solver on multi-core CPUs and GPUs [32]. They balance the factorization loads by organizing the nonzeros of rating matrices.

The SGD solver. Paine *et al.* present an asynchronous SGD to speed up the neural network training on GPUs [18]. In [1, 35], the authors propose a delayed update scheme and a bootstrap aggregation scheme to speed up SGD. `HogWild` uses a lock-free approach to parallelize SGD, that is more efficient than the delayed update scheme [19]. `DSGD` (Distribute SGD) partitions the ratings matrix into several blocks and updates a set of independent blocks concurrently [5]. Kaleem *et al.* show that the parallel SGD can run efficiently on GPU, and their GPU implementation is comparable to a 14-thread CPU implementation [6]. `CuMF_SGD` is a CUDA-enabled SGD solution for large-scale matrix factorization problems, which uses two workload scheduling schemes and a partitioning scheme to utilize multiple GPUs [31]. `Factorbird` uses a parameter server to scale models that exceed the memory of an individual machine, and employs a lock-free learning with a special partitioning scheme to reduce conflicting updates [23]. Sallinen *et al.* present a scalable, communication-avoiding implementation of SGD and demonstrate near-linear scalability on a 14-core system [21].

The SVD solver. The recommendation problem is how to compute a mapping of items and uses to factor vectors [8, 29]. In the collaborative filtering domain, singular value decomposition (SVD) is a well-established technique of identifying latent feature factors. However, the conventional SVD is often inapplicable in matrix factorization of the recommendation field due to the high percentage of missing entries in the sparse user-item matrix. Moreover, overfitting can occur if the sparse matrix is addressed carelessly. Prior works leverage an approach of simply ignoring the missing ratings in the sparse matrix, and directly modeling the observed ratings. Ma proposed four variants of SVD to solve large-scale matrix of collaborative filtering instead of the conventional SVD [2]. They observed that complete incremental learning which updates feature values after scanning a single training score of R, is the best choice for collaborative filtering with millions of training instances. This method minimizes the object function and addresses the negative gradients for each user and item according to each non-zero elements of the R matrix per time. Therefore, it requires a total of nnz iterations.

8 Conclusion

In this work, we have proposed BALS, an efficient implementation of the least squares algorithm for large-scale matrix factorization on GPUs. Through analyzing the algorithm and the recommendation datasets, we observed that there exist many repeated data loads during the ALS factorization. BALS aims to improve the data-moving efficiency across memory hierarchies. At the core of BALS is a new compressed blocked storage format for sparse matrices, which is used to build a blocked ALS implementation. We have further developed a data reordering technique to enhance the data locality. Our experiments reveal that our approach can outperform state-of-the-art implementations. Our implementation generally runs faster than `Gates'` implementation with a speedup of up to 2.08× on K20C, 3.72× on TITAN X and 3.13× on TITAN RTX. `BALS` also outperforms `CDMF`, `cuMF_CCD` and `cuMF_SGD` over different latent feature sizes on K20C. Furthermore, reordering brings another performance improvement of up to 23.68% on K20C, 19.87% on TITAN X and 20.38% on TITAN RTX.

Acknowledgments

The authors would like to thank our anonymous reviewers for their invaluable comments and suggestions. This research was supported by the National Key R&D Program of China under Grant No. 2018YFB0204301, the

National Natural Science Foundation of China under Grant No. 61972408 and 61972415, the Science Challenge Project under Grant No. TZZT2016002, and the Science Foundation of China University of Petroleum, Beijing under Grant No. 2462019YJRC004, 2462020XKJS03.

REFERENCES

[1] A. Agarwal and J. C. Duchi. Distributed delayed stochastic optimization. In *NIPS 2011*.

[2] C. chao Ma. A guide to singular value decomposition for collaborative filtering. 2008.

[3] J. Chen et al. Efficient and portable ALS matrix factorization for recommender systems. In *IPDPS Workshops 2017*.

[4] M. Gates et al. Accelerating collaborative filtering using concepts from high performance computing. In *Big Data 2015*.

[5] R. Gemulla et al. Large-scale matrix factorization with distributed stochastic gradient descent. In *SIGKDD 2011*.

[6] R. Kaleem et al. Stochastic gradient descent on gpus. In *GPGPU@PPoPP 2015*.

[7] K. Kaya et al. Parallelized preconditioned model building algorithm for matrix factorization. In *MOD 2017*.

[8] Y. Koren et al. Matrix factorization techniques for recommender systems. *IEEE Computer*, 2009.

[9] J. Kurzak et al. Implementation and tuning of batched cholesky factorization and solve for nvidia gpus. *IEEE Transactions on Parallel and Distributed Systems*, 2016.

[10] W. Liu. *Parallel and Scalable Sparse Basic Linear Algebra Subprograms*. PhD thesis, University of Copenhagen, 2015.

[11] W. Liu and B. Vinter. Csr5: An efficient storage format for cross-platform sparse matrix-vector multiplication. In *ICS 2015*.

[12] Y. Low et al. Distributed graphlab: A framework for machine learning in the cloud. *PVLDB*, 2012.

[13] Z. Lu, Y. Niu, and W. Liu. Efficient block algorithms for parallel sparse triangular solve. In *ICPP 2020*.

[14] X. Meng et al. Mllib: Machine learning in apache spark. *CoRR*, abs/1505.06807, 2015.

[15] D. K. Nguyen and T. B. Ho. Accelerated parallel and distributed algorithm using limited internal memory for nonnegative matrix factorization. *J. Global Optimization*, 2017.

[16] I. Nisa et al. Parallel ccd++ on gpu for matrix factorization. In *GPGPU 2017*.

[17] Y. Niu, Z. Lu, M. Dong, Z. Jin, W. Liu, and G. Tan. Tilespmv: A tiled algorithm for sparse matrix-vector multiplication on gpus. In *IPDPS 2021*.

[18] T. Paine et al. GPU asynchronous stochastic gradient descent to speed up neural network training. *CoRR*, abs/1312.6186, 2013.

[19] B. Recht et al. Hogwild: A lock-free approach to parallelizing stochastic gradient descent. In *NIPS 2011*.

[20] A. V. Rodrigues et al. Accelerating recommender systems using gpus. In *Applied Computing 2015*.

[21] S. Sallinen et al. High performance parallel stochastic gradient descent in shared memory. In *IPDPS 2016*.

[22] M. T. Schaub et al. Sparse matrix factorizations for fast linear solvers with application to laplacian systems. *SIAM J. Matrix Analysis Applications*, 2017.

[23] S. Schelter et al. Factorbird - a parameter server approach to distributed matrix factorization. *CoRR*, abs/1411.0602, 2014.

[24] U. Simsekli et al. Parallelized stochastic gradient markov chain monte carlo algorithms for non-negative matrix factorization. In *ICASSP 2017*.

[25] G. Takács et al. Scalable collaborative filtering approaches for large recommender systems. *Journal of Machine Learning Research*, 2009.

[26] W. Tan et al. Faster and cheaper: Parallelizing large-scale matrix factorization on gpus. In *HPDC 2016*.

[27] D. Tao et al. Large sparse cone non-negative matrix factorization for image annotation. *ACM TIST*, 2017.

[28] C. Teflioudi et al. Distributed matrix completion. In *ICDM 2012*.

[29] L. Wu and A. Stathopoulos. A preconditioned hybrid svd method for accurately computing singular triplets of large matrices. *SIAM J on Science Computing*, 2015.

[30] X. Xie et al. Cumf_sgd: Parallelized stochastic gradient descent for matrix factorization on gpus. In *HPDC 2017*.

[31] X. Xie et al. Cumf_sgd: Fast and scalable matrix factorization. *CoRR*, abs/1610.05838, 2016.

[32] X. Yang et al. High performance coordinate descent matrix factorization for recommender systems. In *CF 2017*.

[33] H. Yu et al. Scalable coordinate descent approaches to parallel matrix factorization for recommender systems. In *ICDM 2012*.

[34] Y. Zhou et al. Large-scale parallel collaborative filtering for the netflix prize. In *AAIM 2008*.

[35] M. Zinkevich et al. Parallelized stochastic gradient descent. In *NIPS 2010*.

Jing Chen is currently a PhD student in Chalmers University of Technology, Sweden. She received her Master degree in computer science from National University of Defense Technology (NUDT), China, in 2018. Her research interests are energy efficient task scheduling runtime, power modeling, recommender systems and GPU parallel programming.

Jianbin Fang is an assistant professor in computer science at NUDT. He obtained his Ph.D. from the Parallel and Distributed System Group at Delft University of Technology. His research interests include parallel programming for many-cores, parallel compilers, performance modeling, and scalable algorithms.

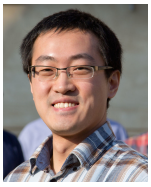

Weifeng Liu is a Full Professor at China University of Petroleum (CUP), Beijing. He received his Ph.D. from the University of Copenhagen, and has been an EU Marie Curie Fellow at the Norwegian University of Science and Technology. He received his B.E. degree and M.E. degree in computer science both from CUP. His research interests include numerical linear algebra, parallel computing and mathematical software.

Canqun Yang is now a full processor in computer science at NUDT. His research interests are performance analysis of high-performance computing systems, parallel compilers, parallel programming, and high-performance computing applications.